Photodissociation of Oxalyl Chloride at 193 nm Probed via Synchrotron Radiation

Naoki Hemmi and Arthur G. Suits*

Chemical Sciences Division, Ernest Orlando Lawrence Berkeley National Laboratory, Berkeley, California 94720

Received: March 3, 1997; In Final Form: April 22, 1997[⊗]

The photodissociation dynamics of oxalyl chloride, $(ClCO)_2$, have been studied at 193 nm using photofragment translational spectroscopy with intense tunable vacuum-UV probe light provided by undulator radiation at the Advanced Light Source. Time-of-flight spectra for *m*/*e* 28 (CO^+), 35 (Cl^+), and 63 ($ClCO^+$) are presented, along with translational energy distributions (P(E)) derived from forward convolution fitting. While the $P(E)$ of ($ClCO^+$) has a single sharp peak, those of (CO^+) and (Cl^+) show quite similar bimodal distributions. These observations suggest that the first step is an impulsive three-body dissociation yielding fast components of CO and Cl and that the remaining ClCO subsequently decomposes to give the slow components. This picture confirms a previous study of the photodissociation of oxalyl chloride at 230 nm using the photofragment imaging technique and provides more insight into the overall dynamics of the process. In addition, the tunable vacuum-UV photoionization has allowed for the measurement of the photoionization efficiency curve for the chloroformyl radical for the first time.

I. Introduction

We recently reported a state-resolved photofragment imaging study of the photodissociation of oxalyl chloride, $(COCl)_2$, in the vicinity of 230nm.[1] In that work, hereafter referred to as I, we presented translational energy and angular distributions for both ground state and spin−orbit excited chlorine atoms, as well as a number of rotational levels of the ground vibrational state of CO. On the basis of the observed distributions, we proposed an unusual dissociation mechanism in which, following the absorption of a photon, a strong impulse occurs between one of the chlorine atoms and one of the CO moieties with the C−C bond breaking simultaneously and with little concomitant momentum transfer to the ClCO fragment. The latter decomposes on a longer time scale yielding, in total, two chlorine atoms and two CO molecules, each showing distinct translational energy and angular distributions. This unusual process, a concerted three-body dissociation followed by secondary decomposition of the ClCO, results in four photofragments arising out of absorption of a single UV photon. This is possible in oxalyl chloride owing to the relatively weak (27 kJ/mol)[2] ClCO bond. However, a number of questions remained. We were unable to detect any chloroformyl radical product in the original imaging experiment since those studies were based on resonant photoionization and no suitable transitions were found for ClCO. In addition, some uncertainties remained in the branching among the various products owing to uncertainties in the relative line strengths for the probe transitions and in the deconvolution of the two different velocity components for the Cl and CO products. Finally, because the CO distributions were measured state-specifically, it was not possible to get the overall translational energy distributions for the CO.

To address these outstanding questions, we have studied the photodissociation of oxalyl chloride at 193 nm using photofragment translational spectroscopy. These studies were performed using universal detection employing undulator radiation on Endstation One at the Chemical Dynamics Beamline at the Advanced Light Source.[3,4] The use of a universal vacuum-UV ionization source has several advantages that are critical to the success of the experiment. One, the use of a cold photon beam rather than a hot filament, allows us to cool the ionization region to 15 K, at the same time providing a very small ionization volume. This allows for the detection of CO, mass 28, with great sensitivity. Furthermore, the use of the soft photoionization as opposed to electron bombardment allows us to detect weakly bound radical products as primary dissociation channels.

Oxalyl chloride has been the subject of extensive ab initio investigations over the past 40 years owing to particular interest in the nature of the internal rotations and the existence and identity of conformers beyond the lowest energy antiform.[5−8] In contrast, the photochemistry of oxalyl chloride has been little studied. UV-induced photoprocesses in argon and xenon matrices were studied using FTIR.[9] UV photodissociation of oxalyl chloride to give CO and phosgene was reported in those studies but not considered in detail. Here we present an investigation of oxalyl chloride dissociation at 193 nm using photofragment translational spectroscopy. These experiments are complementary to the earlier state-resolved imaging experiments presented in I; taken together they demonstrate the power of the combination of state-resolved and universal detection methods to reveal the underlying dynamics.

II. Experimental Section

These experiments were performed using a rotatable source molecular beam apparatus on the Chemical Dynamics Beamline at the Advanced Light Source at Lawrence Berkeley National Laboratory. The apparatus has been described in detail elsewhere.[4,3,10] Briefly, a molecular beam intersects at right angles with a laser, and the photodissociation products are detected by a quadrupole mass spectrometer. The molecular beam source is rotatable to allow data collection at angles of −20 to +110° between the molecular beam and detector. The most significant feature in the experimental setup is the use of the tunable UV undulator radiation for photoionization of the neutral photofragments, in place of the electron impact ionizer. A complete description of the undulator radiation is given in ref 3. For the oxalyl chloride photodissociation studies, the molecular beam was prepared by bubbling helium through oxalyl chloride held at −5 °C, where it has a vapor pressure of

* Author to whom correspondence should be addressed.
[⊗] Abstract published in *Advance ACS Abstracts,* August 1, 1997.

S1089-5639(97)00786-X CCC: $14.00

about 15 Torr with a total stagnation pressure of 600 Torr, yielding a 2.5% beam. The mixture was expanded through a pulsed valve (Gereral Valve) operating at 100 Hz with 500 μs pulses into a source chamber maintained at 10^{-4} Torr. The mean velocity of the beam was 1260 m/s with full width at half-maximum (fwhm) of 15%. After collimation by two skimmers separated by a region of differential pumping, the molecular beam was crossed by the loosely focused output of a pulsed excimer laser (Lambda Physics LPX200) operating at the ArF (193.3 nm) transition with 40 mJ/pulse at a fluence of 500 mJ/cm^2. A fraction of the neutral photofragments recoiled out of the molecular beam traveled into the spot of ionization by the undulator radiation, located 15.1 cm away from the laser interaction region. The undulator radiation is continuously tunable from 5 to 30 eV with a bandwidth of 2.5%, giving an average of 5×10^{15} photons/s at the fundamental. At the point of intersection with the dissociation products, it is focused to 0.15×0.25 mm. The ionized particles are extracted into a quadrupole mass filter and counted by a Daly ion counter.[11] A multichannel scaler, triggered by the laser pulse, was used to record the time-of-flight spectra at various angles between the molecular beam and detector. There are several substantial advantages to the tunable vacuum-UV ionization scheme, compared with the electron impact ionizer. First, ionization energies can be tuned selectively in a wide range according to the ionization potential of the species of interest, precluding dissociative ionization of parent molecules and greatly reducing background. In addition, the small ionization volume provides additional reduction in background signals. Finally, as mentioned above, the "cold" photon beam allows facile cooling of the ionization region to 15 K for very effective cryopumping.

Some small time-dependent background arising from fragmentation of parent molecules in the detector does occur (not laser-dependent), so that for all of the time-of-flight (TOF) spectra presented, shot-to-shot background subtraction was used. The output signal of a pulse generator was split in two pulses. While the first one was used to drive the pulsed valve, the second was frequency divided by 2 with a delay and used to trigger the laser and the multichannel scaler. Operating the pulsed valve at 100 Hz and the laser at 50 Hz and opening a temporal window of 16 ms on the multichannel scaler (4 μs $\times$ 4000 channels), TOF spectra with laser on and off were recorded at the same time and the background was subtracted on alternate shots. The translational energy distributions were obtained by a forward convolution technique. A trial translational energy is convoluted with the instrumental response functions to yield a calculated TOF spectrum in the laboratory reference frame, which is then compared to the experimental one.[12,13] The translational energy distribution is repeatedly adjusted until a good fit is obtained. In all cases presented here the translational energy distributions are reported for each fragment separately.

III. Results and Analysis

Photofragment TOF spectra were collected for *m*/*e* 28 (CO^+) at source angles of 25 and 40°, *m*/*e* 35 (Cl^+) at source angles of 15 and 40°, and *m*/*e* 63 ($ClCO^+$) at source angles of 10 and 20°, shown in Figure 1−3, respectively. For all of the TOF spectra presented, the modulated background was subtracted shot-by-shot, the open circles represent the data, and the solid line is the calculated TOF based on the optimized product translational energy distribution.

For *m*/*e* 28 (CO^+), the TOF spectra were obtained with 10^5 laser shots and 14.5 eV undulator radiation. In Figure 1, it is clear that there is more than one dissociation channel resulting

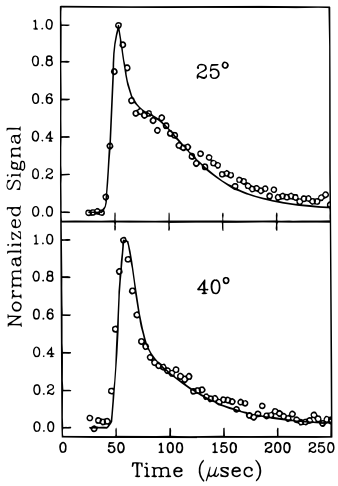

Figure 1. TOF spectra of *m*/*e* 28 (CO^+) at laboratory angles of 25 and 40° with photoionization energy of 14.5 eV. Circles represent the data, and lines are the forward convolution fits using the $P(E)$ in Figure 4A.

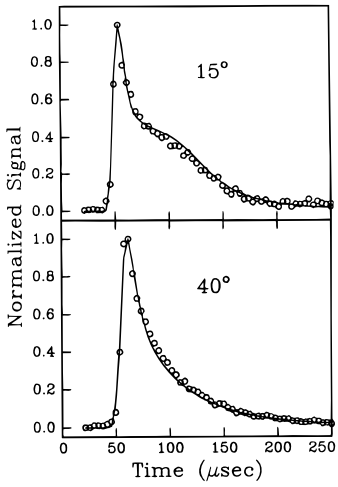

Figure 2. TOF spectra of *m*/*e* 35 (Cl^+) at laboratory angles of 15 and 40° with photoionization energy of 14.0 eV. Circles represent the data, and lines are the forward convolution fits using the $P(E)$ in Figure 4B.

in CO fragments. The data at 25° exhibits the fast component peaked at 55 μs and the slow component showing a clear shoulder near 100 μs. The presence of the fast contribution is clearly seen in the data at 40°. The translational energy distribution yielding the two contributions is given in Figure 4A. For both CO and Cl, the fitting was accomplished in two steps. Initially, the TOF spectra were all fitted by assuming an isotropic angular distribution. From this it became clear that the distributions were bimodal, just as had been observed in dissociation at 230 nm; furthermore, the translational energy distributions were quite similar. On this basis, we decomposed the distributions into distinct fast and slow components using the same form for these that we had employed in analyzing the imaging results. In a second step, we fed those distributions back into the simulation program for further fine tuning of both the distributions and the relative contributions of the fast and slow components. In the second step, the photofragment angular distributions were assumed to be the same as in the experiments at 230 nm: isotropic ($\beta = 0$) for both slow components; $\beta = 0.4$ for the fast CO and $\beta = 0.8$ for the fast Cl. This led to a small shift (5%) in the relative branching inferred between the slow and fast components when compared to the fit assuming both components possess isotropic angular distributions. For CO the relative contributions obtained are 37% slow and 63%

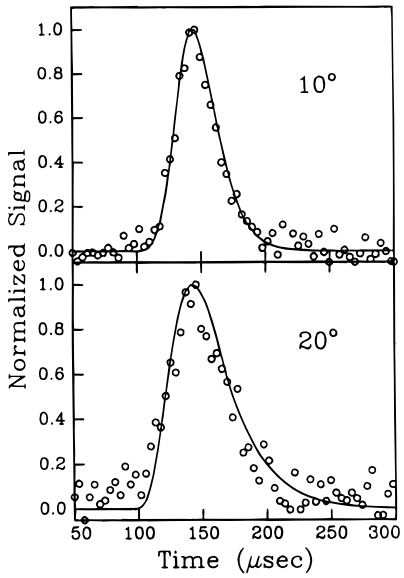

Figure 3. TOF spectra of *m*/*e* 63 ($ClCO^+$) at laboratory angles of 10 and 20° with photoionization energy of 14.5 eV. Circles represent the data, and lines are the forward convolution fits using the $P(E)$ in Figure 4C.

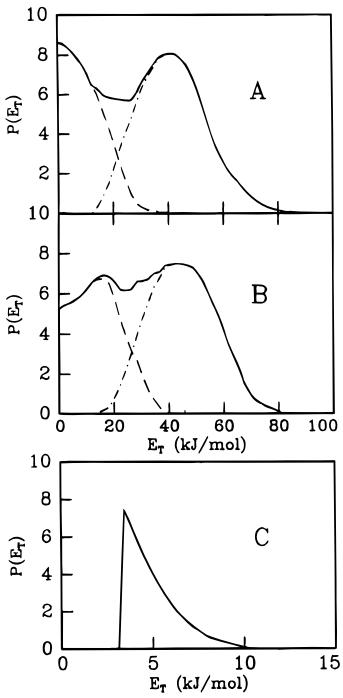

Figure 4. Center-of-mass translational energy distributions (A) for *m*/*e* 28 (CO^+), (B) for *m*/*e* 35 (Cl^+), and (c) for *m*/*e* 63 ($ClCO^+$). Dashed lines represent the slow components, dotted−dashed lines are the fast contribution, and the solid line is the sum of these.

fast. The uncertainties in these values are large because of the range of possible approaches in decomposing the two contributions; however, in the imaging experiment we were guided by the spin−orbit excited Cl, which showed exclusively the fast component. This gives us some assurance about the shape of the distribution we are using to fit that component, which correspondingly constrains all of the fitting described here. While the slow dissociation channel is peaked near zero, the fast channel is peaked at 45 kJ/mol and extends to around 80 kJ/mol. For CO, the average energy release in the slow component is 10.7 kJ/mol; in the fast component it is 41.7 kJ/mol; the total average translational energy in CO is 30.2 kJ/mol.

For *m*/*e* 35 (Cl^+), the TOF spectra were obtained with 7×10^4 laser shots and 14.0 eV undulator radiation. In Figure 2, in a similar fashion to the *m*/*e* 28 (CO^+) TOF spectra, there can be seen two dissociation channels resulting in Cl fragments. The data at 15° indicate the fast component peaked near 60 μs and the slow component showing a broad shoulder at 100 μs. The presence of the fast contribution is also confirmed in the data at 40°. The translational energy distribution yielding the two contributions is given in Figure 4B, fitted as described above. For the Cl fragment, the relative contributions obtained were 41% for the slow component and 51% for the fast component (c.f. 37% slow and 63% fast for CO). These are certainly equivalent within the range of uncertainty in the analysis. The average energy in the slow Cl was 14.5 kJ/mol, and in the fast Cl, 46.0 kJ/mol. The total translational energy in Cl was 33.1 kJ/mol.

For *m*/*e* 63 ($ClCO^+$), TOF spectra were observed with 10^5 laser shots and 14.5 eV undulator radiation. In Figure 3, in contrast to the *m*/*e* 28 (CO^+) and 35 (Cl^+) TOF spectra, there is only one dissociation channel resulting in ClCO fragments. The data at both 10 and 20° show a single peak near 145 μs. The translational energy distribution yielding the single contribution is given in Figure 4C, which shows a small and narrow peak at low energy. The sharp edge of the lower energy side indicates that ClCO radical with low velocity does not survive and is decomposed into CO and Cl. The minimum translational energy observed is about 4.0 kJ/mol, and the average energy is 4.6 kJ/mol. ClCO products with energies down to 1.5 kJ/mol should be within the range of the detector at 10°. On the basis of the fitting of the Cl and CO above, if we assume the fast component must equal the slow component except for that portion that remains bound as ClCO, we can estimate the fraction of ClCO that remains bound. From the analysis of the CO, we find 21% of the ClCO might remain bound, while from the Cl analysis the fraction is 15%, giving an average of 18%. Again, these values are within the range of uncertainty associated with the analysis.

The photoionization efficiency curve for the ClCO radical was measured by integrating the TOF signal at *m*/*e* 63 ($ClCO^+$), taken at a source angle of 15° as a function of the photoionization energy from 10 to 14.5 eV. The results are presented in Figure 5, showing a threshold of 11.5 ± 0.3 eV.

Power dependence studies showed a linear or less than linear dependence of the Cl product at the fluences employed in these experiments, implying that the observed spectra arise from one-photon events. However, the possibility of multiphoton dissociation processes may be rejected simply on the basis of the translational energy release. Were the ClCO to absorb an additional 193 nm photon, for example, some fraction of the Cl and CO products would inevitably have translational energies far greater than those observed.

IV. Discussion

These observations suggest a simple picture of the dissociation dynamics similar to that proposed for photodissociation of oxalyl chloride at 230 nm:[1] the multiple bond-breaking processes for oxalyl chloride consist of two dissociation steps. The first step is an impulsive three-body dissociation,

$$(ClCO)_2 \rightarrow CO + Cl + ClCO \qquad (1)$$

which yields fast CO, Cl, and chloroformyl radical ClCO. The measured distributions imply that little mometum is transferred to the ClCO in this step, with the impulse along the Cl−C bond. In the second step, most of the remaining ClCO undergoes

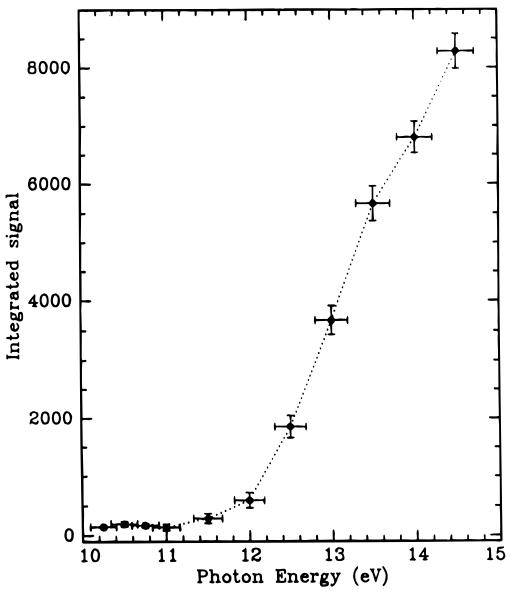

Figure 5. Photoionization spectrum of *m/e* 63 ($ClCO^+$) photofragments from oxalyl chloride at a source angle of 15° for undulator radiation energies of 10.1−14.5 eV. The vacuum-UV had a roughly Gaussian bandwidth of 0.5 eV fwhm.

subsequent decomposition,

$$ClCO \rightarrow CO + Cl \qquad (2)$$

which yields slow CO and Cl. As suggested by the fast components of TOF spectra in Figures 1 and 2, free fragments CO and Cl seem to be dynamically linked; that is, it is likely to break both the C−C and Cl−CO bonds simultaneously, given by (1). The direct observation of ClCO here confirms it as a primary product, and the translation energy distributions in Figure 4C show clearly that there is no fast contribution in that product, consistent with the picture we have outlined.

In the imaging experiments reported in I, state-resolved distributions were obtained for both ground state and spin−orbit excited chlorine atoms with the branching between these two hinging upon measurements of the relative line strengths for the REMPI transition used in the detection.[1] The present results yield a total translational energy distribution for all chlorine atoms, so they are free of uncertainties arising from spectroscopic considerations. Similarly, the previous study was able to determine translational energy distributions for particular rotational levels of CO $v = 0$, but the total CO translational energy distribution could not be directly determined. Further, contributions from higher vibrational levels of CO were largely undetermined. Nevertheless, in fitting the time-of-flight spectra for Cl and CO here and deconvoluting the fast and slow contributions, we have relied on the measurements made in the imaging experiments both (a) to determine independent angular distributions for the fast and slow components which are then used in fitting these components independently and (b) to determine the translational energy distribution for the fast component, which we were able to do in the imaging experiment because the spin−orbit excited Cl arose almost entirely from the fast channel, as we have indicated above. The energy distributions, as well as the branching between the fast and slow components, are very similar to those obtained in the imaging experiments. In fact, the fast component is a bit narrower in the present experiment. This is likely owing to the fact that the energy distribution determined from the imaging experiment is a direct deconvolution which includes some experimental broadening, whereas the energy distribution determined here is the input to a forward convolution over the experimental perimeters and hence contains no experimental broadening. It is perhaps surprising that the energy release is so similar at 193 and 230 nm. Certainly this implies that the same electronic transition is involved. It is generally believed that the transition is $\pi \rightarrow \pi^*$, which then couples to the $n \rightarrow \sigma^*$ surface.[14−17] Based upon the similarities in the distributions at 230 and 193 nm, it seems likely that the translational energy release arises from the magnitude of the repulsion at the crossing of the surfaces.

The ClCO peaks at very low energy consistent with the above picture of a little momentum transfer to that species. In addition, the range of the translational energy distribution is consistent with the very weak (27 kJ/mol) Cl−CO bond. In addition to observing this as a primary photodissociation product, the use of the tunable vacuum-UV allows us to record a photoionization efficiency curve for this radical for the first time. Given uncertainties in the energy width of the undulator radiation and uncertainty in determining the ionization onset, we give an ionization potential (IP) of 11.5 ± 0.3 eV for this radical. In fact this is an upper bound: since the ClCO cannot possess more than 25 kJ/mol internal energy (since this would exceed the bond energy) the IP is not likely to be higher than the observed threshold, but the Franck−Condon factors are not known, so that the true IP could be somewhat lower and the shape of the curve could be different for a completely cold sample.

The photon energy at 193 nm is 619 kJ/mol, and assuming a C−C bond energy of 322 kJ/mol and Cl-CO bond energy of 25 kJ/mol,[2] the total available energy is about 247 kJ/mol (619 - 322 - 2 × 27 = 243 kJ/mol). An average of 105 kJ/mol or 43% was released into translation. This implies an additional 130 kJ/mol in internal degrees of freedom of CO, after accounting for a small amount in electronic excitation of the spin−orbit excited Cl. This implies both a more excited rotational distribution than that seen at 230 nm (which peaked at $J = 30$) but, more significantly, a substantial population of vibrationally excited CO.

V. Conclusion

We have studied the photodissociation dynamics of oxalyl chloride, $(ClCO)_2$, using photofragment translational spectroscopy with an intense tunable vacuum-UV probe light provided by undulator radiation at the Advanced Light Source. The observations suggest that the first step is an impulsive three-body dissociation yielding fast components of CO and Cl and that the remaining ClCO subsequently decomposes to give the slow components. The results confirm a previous study at 230 nm using the photofragment imaging technique and provide a broad view of the overall dynamics of the process. The use of this universal technique allows for complementary insights into the dynamics when contrasted with the previous photofragment imaging study. In addition, in this experiment, the tunable vacuum-UV photoionization has allowed for the measurement of the phoionization efficiency curves for the chloroformyl radical for the first time.

Acknowledgment. We thank David Blank for valuable assistance and comments on the manuscript. Excellent support by the ALS staff is also acknowledged. This work was supported by the Director, Office of Energy Research, Office of Basic Energy Sciences, Chemical Sciences Division of the U.S. Department of Energy under Contract No. DE-ACO3-76SF00098.

References and Notes

(1) Ahmed, M.; Blunt, D.; Chen, D.; Suits, A. G. *J. Chem. Phys.* **1997**, *106*, 7617.

(2) Lim, K. P.; Michael, J. V. *J. Phys. Chem.* **1994**, *98*, 211.

(3) Heimann, P. A.; Koike, M.; Hsu, C. W.; Evans, M.; Ng, C. Y.; Blank, D.; Yang, X. M.; Flaim, C.; Suits, A. G.; Lee, Y. T. *Proc. SPIE* **1996**, *90*, 2856.

(4) Yang, X.; Blank, D. A.; Lin, J.; Heimann, P. A.; Wodtke, A. M.; Lee, Y. T.; Suits, A. G. In *Synchrotron Radiation Techniques in Industrial, Chemical and Materials Science;* Amico, D., Ed.; Plenum Press: New York, 1996. Yang, X.; Blank, D. A.; Lin, J.; Suits, A. G.; Lee, Y. T.; Wodtke, A. M. *Rev. Sci. Instrum.*, in press.

(5) Saksena, B.; Kagarise, R. *J. Chem. Phys.* **1951**, *19*, 99.

(6) Hassett, D.; Hedberg, K.; Marsden, C. *J. Phys. Chem.* **1993**, *97*, 4670.

(7) Danielson, D.; Hedberg, L.; Hedberg, K.; Hagen, K.; Traetteberg, M. *J. Phys. Chem.* **1995**, *99*, 9374.

(8) Durig, J.; Davis, J.; Wang, A. *J. Mol. Struct.* **1996**, *375*, 67.

(9) Schroeder, W.; Monnier, M.; Davidovics, G.; Allouche, A.; Verlaque, P.; Pourcin, J.; Bodot, H. *J. Mol. Struct.* **1989**, *197*, 227.

(10) Blank, D. A.; North, S. W.; Stranges, D.; Suits, A. G.; Lee, Y. T. *J. Chem. Phys.* **1996**, *106*, 539.

(11) Lee, Y. T.; McDonald, J. D.; LeBreton, P. R.; Herschbach, D. R. *Rev. Sci. Instrum.* **1969**, *40*, 1402.

(12) Wodtke, A. M. Ph.D. thesis, University of California, Berkeley, 1986.

(13) Zhao, X. Ph.D. thesis, University of California, Berkeley, 1988.

(14) Person, M. D.; Kash, P. W.; Butler, L. J. *J. Phys. Chem.* **1992**, *96*, 2021.

(15) Person, M. D.; Kash, P. W.; Butler, L. J. *J. Chem. Phys.* **1992**, *97*, 355.

(16) North, S. W.; Blank, D. A.; Geseltzer, J. D.; Longfellow, C. A.; Lee, Y. T. *J. Chem. Phys.* **1995**, *102*, 4447.

(17) Lane, I. C.; Meehan, R.; Powis, I. *J. Phys. Chem.* **1995**, *99*, 12371.